Research article Available online www.ijsrr.org ISSN: 2279–0543

International Journal of Scientific Research and Reviews

Influence of Bi-doping on the structure and efficiency of TiO_2 photoanodes

Mohamed H. Badr[1*], Ahmed A. El-Hamalawy[2], M. M. El-Kholy[3] and Alshimaa Ali[4]

[1,2,3,4] Menoufia University, Faculty of Science, Physics Department, Shebin El-Kom 32511, Egypt.

ABSTRACT

Bismuth-doped TiO_2 photoanodes of dye sensitized solar cells were synthesized by using powder bismuth oxide. The effect of bismuth doping on the crystallite size, strain lattice distortion and crystallinity of titanium oxide was investigated and its influence on the photovoltaic behavior of dye sensitized solar cells was studied. The variation in short-current density and open-circuit voltage with Bi-doping was explained in terms of changes in both electron-hole recombination and conduction band edge of titanium oxide, respectively. The prepared photoanodes were characterized by X-ray diffraction and energy dispersive X-ray analyses.

KEYWORDS: Bi-doping, crystal structure, DSSC, X-ray diffraction.

,

***Corresponding Author**

Mohamed H. Badr

Menoufia University, Faculty of Science, Physics Department,

Shebin El-Kom 32511, Egypt.

Phone: 002-010-96296262

Email*: mhbadr0@hotmail.com

INTRODUCTION

It is expected that conventional solar cells will be replaced by Dye Sensitized Solar Cells (DSSCs) due to their low cost and simple manufacturing processes[1,2]. Basically, a DSSC consists of photoanode (wide band gap semiconductor oxide(s) on transparent conducting glass), sensitizer, redox electrolyte and counter electrode. Considerable efforts have been devoted on all of these constituents to increase the overall efficiency of DSSC devices. Many studies focus on improving the performance of photoanodes have been published, see for example Refs. [3,6]. More than a few of these studies employed TiO_2 semiconductor because of its high efficiency, low cost, chemical inertness and photostability[7,8].

The electronic properties of TiO_2 can be modified by doping, either by replacing the Ti^{4+} cation or the O^{2-} anion[9]. There are different ways for entering the dopant into the TiO_2-lattice, e.g., mixing TiO_2 precursor solution with the dopant precursor and doping TiO_2 electrochemically by dissolving the dopant in the electrolyte solution[10]. Moreover, coating the photoanodes with another wide band gap semiconductors (such as Al_2O_3, ZnO, ZrO_2 and Nb_2O_5) to reduce charge recombination were reported[11-14]. Doping TiO_2 photoanodes with Nb[15] and Sb[16] improved the performance of DSSCs due to enhancement of the short-circuit current density. Furthermore, metal doping of TiO_2 with Sn, Zn and W exhibited a positive shift in the conduction band edge that increased the electron injection efficiency and suppressed the carrier recombination[15,17]. Nonmetals such as nitrogen, fluorine, carbon and sulfur also shifted the TiO_2 conduction band edge and decreased the concentration of oxygen vacancies, consequently, reduced the trapping at the defect sites[18]. Rare-earth-doping has been the subject of extensive research as well, e.g. Hafez et al.[19] studied the effect of Eu and Sm doping on the efficiency of DSSCs. On the other hand, cocktail of bi-semiconductors such as TiO_2 and Fe_2O_3 were used in the photoanode material and resulted in increasing the performance of the DSSC due to the combined conduction bands[20]. Moreover, photoanodes based on bismuth oxide with β-Bi_2O_3 morphology prepared by chemical bath deposition method was reported[21]. The DSSC efficiency was enhanced by suppressing charge recombination when another ZnO layer was applied. Bismuth-TiO_2 photoanodes were synthesized mostly via sol–gel method, see for example Refs.[22, 23].

In this work, we employed powder bismuth oxide via a simple mechanochemical route to dope TiO_2 photoanodes as $(Bi_2O_3)_x$-$(TiO_2)_{1-x}$ with x=0.0, 0.10 and 0.15. To the extent of our knowledge, there is no reported work on doping titanium oxide with powder bismuth oxide. The employed TiO_2 was prepared as nanoparticles and the used Bi_2O_3 has the most stable monoclinic α-phase[24]. The crystal structure of photoanodes with different doping rations was investigated by

XRD and EDX. Also, the Bi-doping influence on the photovoltaic efficiency of DSSC devices was studied.

MATERIALS AND METHODS

Materials

Chemical materials of titanium dioxide (TiO_2: BHD, 98.0%), Bismuth (III) oxide (Bi_2O_3: Loba Chemie ,99%), acetylacetone ($CH_3.CO.CH_2.CO.CH_3$: Loba Chemie, 98.0%), triton X-100 ($C_{34}H_{62}O_{11}$: El-goumhouria), Hydrochloric acid (HCl: Elnaser pharm. chem., 30.0-34.0%), Hydrogen peroxide (H_2O_2: PubChem, 50.0%), amonia solution (NH_3: Elnaser pharm. chem., 33.0%), titanium tetrachloride ($TiCl_4$: Loba Chemie, 99.5%), hydrogen hexachloroplatinate (IV) solution **(**H_2PtCl_6: Sigma Aldrich), absolute ethanol (C_2H_5OH: Honeywell), pure acetone (CH_3COCH_3: Elnaser pharm. chem.), isopropyle-alcohol **(**$(CH_3)_2CHOH$: Elnaser pharm. chem.), ethylene glycol ($C_2H_6O_2$: S. D. Fine-Chem Ltd.), iodine resublimed (I_2: Elnaser pharm. chem.), potassium iodide (KI: Elnaser pharm. chem., 99.5%), N719 dye (Di-tetrabutylammonium cis-bis(isothiocyanato)bis(2,2'-bipyridyl-4,4'-dicarboxylato) ruthenium(II): Dyesol) were used. Also, Fluorine-doped SnO_2 (FTO: 2.2-mm thick, 14Ω/sq., Pilkington) was utilized as our transparent conducting oxide (TCO) glass.

Preparation of TiO_2 nanoparticles

25 gm of raw TiO_2 was added to a solution of 25 ml of HCl, 50 ml of H_2O, 12.5 ml of H_2O_2 and 6.25 ml of NH_3 and stirred for 17 h to get a white suspension. Then, the suspension was washed and precipitated by repeated cycles of using distilled water and centrifuge. Lastly, the formed precipitate was dried at 70 ^oC for 21 h to get TiO_2 nanoparticles.

Preparation of undoped and Bi-doped TiO_2 pastes

A white solution was made by adding 10 ml of distilled water to 2 ml of $TiCl_4$ in an ice bath and kept under stirring until it became colorless. Then, 3 gm of prepared TiO_2 nanoparticles was added to another beaker with 0.05 ml of triton X-100, 0.1 ml of acetylacetone and 3 ml of distilled water. Lastly, 1.0 ml of the prepared colorless solution was added and the final solution was kept under continuous stirring for 24 h to obtain the TiO_2 paste. To prepare $(Bi_2O_3)_x$-$(TiO_2)_{1-x}$ paste with x= 0.10 and 0.15, bismuth oxide powder was mixed with the previously prepared TiO_2 nanopowder and rigorously ground to facilitate mechanochemical reaction to take place, then the mixed powder followed the same procedure mentioned above for the preparation of TiO_2 paste.

Preparation of electrolyte and Pt layer

To prepare the electrolyte, about 0.6 gm of I_2 was dissolved in 50 ml of ethylene glycol and kept under stirring for 2 h. Then, 4 gm of KI was added to the mixture under continuous stirring for another 2 h and the obtained solution was stored in tight and dark glass container. To prepare the Pt layer of the counter electrode, 20 ml of pure ethanol was added to a beaker containing 0.5 ml of H_2-Hex-Pt (IV). The acquired solution was dispersed on the FTO substrates and gradually heated to 450 ^oC for 30 minutes.

Preparation of film electrodes and DSSCs devices

The prepared paste was spread on the transparent conducting glass using doctor -blade technique and then sintered at 450 ^oC for 30 min. Subsequently, the film was soaked in ethanol solution of N-719 dye for 24 h at room temperature and then gently washed by ethanol. The DSSC devices were assembled and the electrolyte was introduced into the aperture by repeated addition of electrolyte drops (on a hole in the counter electrode) and air suction to ensure complete filling of the aperture.

Measurements and characterization

X-ray diffraction (XRD) of $(TiO_2)_{1-x}(Bi_2O_3)_x$ working electrodes was recorded by using TMR (APD 2000 Pro) diffractometer with Cu-$K_{\alpha 1}$ radiation (λ = 1.54056 Å) with 2θ covering the range from 20^o to 70^o with an angular resolution of 0.03^o. The elemental analysis was carried out by using EDX (Energy Dispersive X-ray analysis) unit attached to SEM model Quanta 250 FEG (Field Emission Gun). The J-V curves of DSSCs were measured by using current amplifier (Kiethley 427), multimeter (Aplab 1087) and data acquisition (DataQ: DI-158U). The DSSCs devices were irradiated with a homemade solar simulator with xenon lamp (35 W), halogen lamp (55 W) and equipped with IR and UV filters to irradiate a DSSC active area of 0.35 cm^2. The power density of the simulator was 55 mW/cm^2 (measured by using SPM-1116SD Lutron solar power meter) which corresponds to a solar power of about 19 mW for the working active area.

RESULTS AND DISCUSSION

X-ray diffraction (XRD) patterns of $(Bi_2O_3)_x$-$(TiO_2)_{1-x}$ with x=0.00, 0.10 and 0.15 photoanodes and powder Bi_2O_3 were shown in Figure 1. Also, the standard diffraction patterns of SnO_2 and TiO_2 rutile and anatase phases were given[25]. All charts were normalized and shifted for clarity purposes. The chart of the raw bismuth oxide powder was compared with standard charts and all given peaks matched the peak positions and relative intensities of standard monoclinc (α-

phase) Bi_2O_3, as referenced in JCPDS 76-1730. All shown diffraction peaks of x= 0.0 photoanode represent pure anatase-TiO_2 phase, in addition to tin oxide (due to FTO: fluorine-doped tin oxide conducting layer) diffraction peaks. It is worth mention that, the small peak at 33.8° belongs to SnO_2 rather than the monoclinc Bi_2O_3. Before we proceed with XRD discussion for Bi-doped samples, we recall that we applied mechanochemical route in preparing the samples. This method is

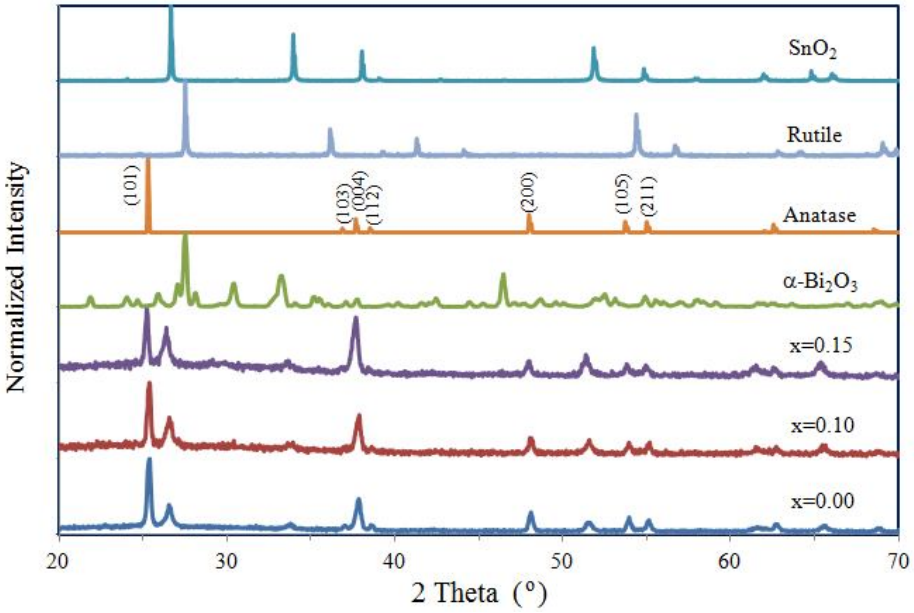

Fig. 1: XRD pattern spectra of $(Bi_2O_3)_x$-$(TiO_2)_{1-x}$ photoanodes for x = 0.0, 0.10 and 0.15 and powder Bi_2O_3. Standard diffraction patterns of SnO_2, rutile and anatase phases of TiO_2 were given.

superior to both liquid phase processes and solid state reaction as it gives finer particle sizes by using low cost raw materials and without the need to high sintering temperatures[26]. Ohara et al.[27] prepared $BiTiO_3$ with particle size of 22 nm by using mechanochemical procedure by ball-milling TiO_2 and $BaCO_3$ powders for 10 min. The reported XRD chart showed the absence of TiO_2 and $BaCO_3$ peaks and only $BiTiO_3$ peaks were observed. Now, the fact that our XRD chart for x= 0.0 represents pure TiO_2 (anatase phase) photoanode is confirmed by the absence of all Bi_2O_3 and rutile peaks; especially major diffractions. This argument is actually applied for Bi-doped photoanodes (x= 0.15 an x= 0.15) as well, where neither Bi_2O_3 nor rutile peaks were observed. The effects of Bi-doping were observed in the shift of peaks toward lower 2θ angle and the gradual decrease of TiO_2 (200) diffraction intensities with the increase of x. Figure 2 showed the observed shift of the major TiO_2 (101) diffraction peak where it shifted from 2θ= 25.37° for undoped sample to 2θ= 25.19° for x= 0.15. This shift suggested an increase in the unit cell volume with increasing of x. Table 1 listed the calculated distortion, $\delta(a/c)$%, of TiO_2 lattice for Bi-doped samples, whereas:

$\delta(a/c) = (a/c)-(a_o/c_o)$

where (a/c) and (a_o/c_o) are the ratios between lattice parameters of Bi-doped and undoped samples, respectively. As observed, the calculated distortion increased with increasing of Bi-doping. On the other hand, we should take in account that there is no evidence of Bi_2O_3 phase in Bi-doped samples, as mentioned above, and the fact that the ionic radius of Bi^{3+} (0.103 nm) is greater than that of Ti^{4+} (0.061 nm) [28]. These facts imply that Bi^{3+} ions substituted Ti^{4+} sites leading to an

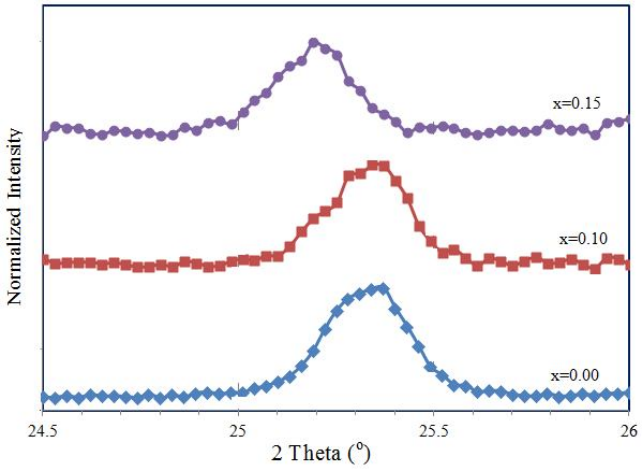

Fig. 2: XRD major TiO_2 (101) diffraction peak of photoanodes for x = 0.0, 0.10 and 0.15.

increase in unit cell volume and absence of any Bi-based phases. Furthermore, the size of the crystallites (D) for different values of x was calculated by using Scherrer formula for the major (101) diffraction peak, as given in Table 1. The reported minute decrease in the average crystallite size with increasing of x could be attributed to growth suppression of similar TiO_2 crystallites due to Bi^{3+} ions doping. In other words, the mismatch between Bi^{3+}-free unit cells and bigger cells with Bi^{3+} ions substituted Ti^{4+} sites decrease the possibility of crystallite growth, i.e. the more the Bi-doping the smaller the crystallite size. Moreover, let us study the effect of Bi-doping on the crystallinity of TiO_2 by considering the peak at about $2\theta = 48.1^o$ with (200) diffraction plane. As seen, this peak undoubtedly refers to TiO_2 (anatase phase) and its intensity decreased with the increasing of Bi-content, x. Therefore, Bi-doping resulted in a decrease in crystallinity of TiO_2 as confirmed by the observed gradual decrease in the intensity of this peak with increasing of x.

Energy-Dispersive X-ray (EDX) spectroscopy was employed to elementally analyze the composition of $(Bi_2O_3)_x$-$(TiO_2)_{1-x}$ photoanodes. Figure 3 showed peaks corresponding to titanium, bismuth, oxygen and carbon indicating the absence of impurities in the prepared photoanodes. The presence of carbon is due to coating of samples with such conducting element. The calculated

content of bismuth in Bi-doped samples were tabulated in Table 1 and agrees fairly well with the starting stoichiometry, x, of $(Bi_2O_3)_x$-$(TiO_2)_{1-x}$ photoanodes.

Table No. 1: "Crystallite size (D), lattice parameters, lattice distortion and EDX analysis of photoanodes"

x	D (nm)	a (Å)	c (Å)	δ (%)	x (EDX)
0.0	33	3.7739	9.5069	0	0.0
0.10	31	3.7794	9.4996	0.0879	0.09
0.15	30	3.8019	9.5505	0.1112	0.14

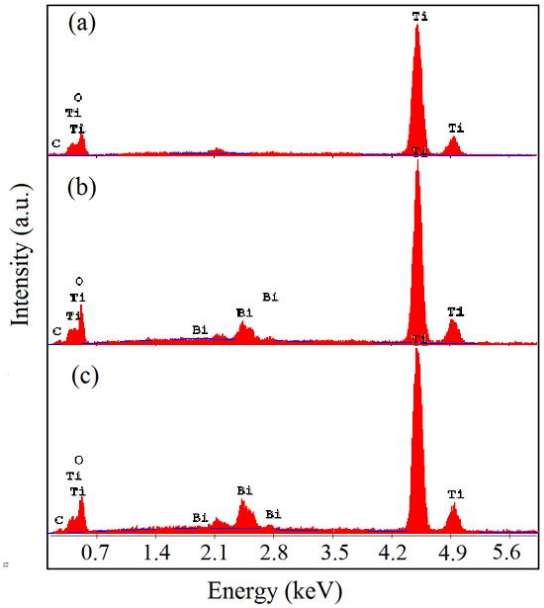

Fig. 3: SEM-EDX analysis of $(TiO_2)_{1-x}$–$(Bi_2O_3)_x$ photoanodes for (a) x= 0.0, (b) x= 0.10 and (c) x= 0.15.

The photocurrent density-voltage curves (J-V) of DSSCs with different Bi-doping concentrations of TiO_2 photoanodes are shown in Figure. 4. The photovoltaic parameters were calculated and tabulated in Table 2. The values of the fill factor (*FF*) for DSSCs with different concentrations of the dopant were calculated and indicated in Table 1. This parameter is a measure of the ideality of a solar cell and is given as:

$$FF = J_{max} V_{max} / J_{sc} V_{oc}$$

where J_{max} and V_{max} are the current density and voltage corresponding to the maximum output power (P_{max}) of the P-V curves and given in Table 2. As observed, both short-circuit current density (J_{sc}) and open-circuit voltage (V_{oc}) were decreased with increasing of Bi-doping, x.

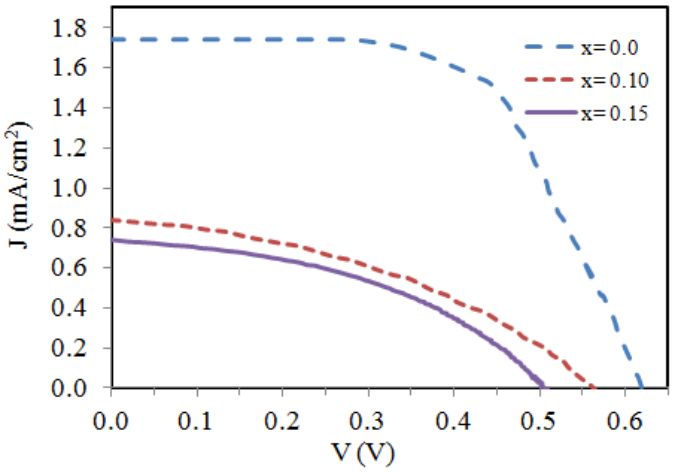

Fig. 4: Current density-voltage curves of $(Bi_2O_3)_x$-$(TiO_2)_{1-x}$ DSSCs for x= 0.0, 0.10 and, 0.15.

Table No. 2: "Parameters of DSSCs with $(Bi_2O_3)_x$-$(TiO_2)_{1-x}$ photoanodes for x= 0.0, 0.10 and 0.15"

x	V_{oc} (V)	J_{sc} (mA/cm^2)	P_{max} (mW)	*FF* (%)	η
0.00	0.62	1.75	0.236	62.3	1.23
0.10	0.56	0.84	0.067	40.6	0.35
0.15	0.51	0.74	0.057	43.0	0.30

Consequently, the light-to-electrical energy conversion efficiency (η) of doped DSSC devices is lower than that of undoped cells, see Table 1. The efficiency (η) was calculated according to the following equation:

$$\eta = P_{max} / P_{in} = J_{sc}\ V_{oc}\ FF / P_{in}$$

where P_{in} is the input power of the incident light on the active area of the cell. The observed decrease in J_{sc} with Bi-doping could be attributed to reduction in TiO_2 crystallinity, as discussed above. This decrease in crystallinity of anatase-TiO_2 phase causes an increase in electron-hole recombination due to reduction in the speed of electrons[22]. Therefore, the observed gradual decrease in current density with increasing of x (Fig. 4) could be attributed to loss of photo-generated electrons by electron-hole recombination processes. To clarify the reduction in V_{oc} with Bi-doping (Fig. 4), let us recall that the measured V_{oc} is the difference between two potentials, namely, the Nernstian potential of the electrolyte and the quasi-Fermi level of TiO_2 [29]. Since conduction bands of TiO_2 and Bi_2O_3 with respect to the absolute vacuum scale are -4.21 eV and -4.83 eV [30], respectively, then the former conduction band is higher than the later. Moreover, the substitution of Ti^{4+} by Bi^{3+} is expected to shift-down the quasi-Fermi level of TiO_2. Consequently,

the effect of increasing Bi-doping of TiO_2 photoanodes is expected to gradually shift-down its conduction band edge and accordingly V_{oc} decreases.

CONCLUSION

We employed powder bismuth oxide to prepare $(Bi_2O_3)_x$-$(TiO_2)_{1-x}$ photoanodes with x= 0.0, 0.10 and 0.15. XRD analysis showed that the prepared titanium oxide nanoparticles have a size of 33 nm with a pure anatase phase. Also, Bi-doping caused distortion in TiO_2 lattice and a reduction in both crystallite size and crystallinity as Bi^{3+} ions substituted Ti^{4+}. The photocurrent density-voltage curves of DSSCs revealed that both short-circuit current density and open-circuit voltage were decreased with increasing of x. The decrease in current density was attributed to an increase in electron-hole recombination associated with the observed reduction in TiO_2 crystallinity. Finally, the observed decrease in open-circuit voltage with increasing Bi-doping was explained in terms of a shift-down of the conduction band edge of titanium oxide.

REFERENCES

1. Oregan B, Gratzel M. A low-cost, high-efficiency solar cell based on dye-sensitized colloidal TiO_2 films. Nature 1991; 353: 737–40.
2. Chiba Y, Islam A, Watanabe Y et al. Dye-Sensitized Solar Cells with Conversion Efficiency of 11.1%. Jpn. J. Appl. Phys. 2006; 45: L638-40.
3. Tahcan Z, Zaban A, Ruhle S. Dye-sensitized solar tubes: A new solar cell design for efficient current collection and improved cell sealing. Sol. Energ. Mat. Sol. Cells. 2010; 94: 317-22.
4. Wang DA, Yu B, F. Zhou, Wang CW, Liu WM. Synthesis and characterization of anatase TiO_2 nanotubes and their use in dye-sensitized solar cells. Mater. Chem. Phys. 2009; 113: 602-06.
5. Pan K, Zhang QL, Liu ZY et al. The photoelectrochemical properties of dye-sensitized solar cells made with TiO2 nanoribbons and nanorods. Thin Solid Films. 2007; 515: 4085-91.
6. Schlichthorl G, Huang SY. Sprague J, Frank AJ. Edge Movement and Recombination Kinetics in Dye-Sensitized Nanocrystalline TiO_2 Solar Cells: A Study by Intensity Modulated Photovoltage Spectroscopy. J. Phys. Chem. B. 1997; 101: 8141-55.
7. Park NG, Lagemaat J, Frank AJ. Comparison of Dye-Sensitized Rutile- and Anatase-Based TiO_2 Solar Cells. J. Phys. Chem. B. 2000; 104: 8989–94.
8. Im JS, Yun J, Lee SK, Lee Y-S. Effects of multi-element dopants of TiO_2 for high performance in dye-sensitized solar cells. J. Alloy Compd. 2012; 513: 573-79.

9. Hoye RLZ, Musselman KP, MacManus-Driscoll JL. Research Update: Doping ZnO and TiO_2 for solar cells. APL Mater. 2013; 1: 060701-11.
10. Roose B, Pathak S, Steiner U. Doping of TiO_2 for sensitized solar cells. Chem. Soc. Rev. 2015; 44: 8326-49.
11. Prasittichai C, Hupp JT. Surface Modification of SnO_2 Photoelectrodes in Dye-Sensitized Solar Cells: Significant Improvements in Photovoltage via Al_2O_3 Atomic Layer Deposition. J. Phys. Chem. Lett. 2010; 1: 1611-15.
12. Seo HO, Park SY, Shim WH, Kim KD et al. Ultrathin TiO_2 Films on ZnO Electron-Collecting Layers of Inverted Organic Solar Cell. J. Phys. Chem. C. 2011; 115: 21517-20.
13. Li TC, Goes MS, Fabregat-Santiago F et al. Surface Passivation of Nanoporous TiO_2 via Atomic Layer Deposition of ZrO_2 for Solid-State Dye-Sensitized Solar Cell Applications. J. Phys. Chem. C. 2009; 113: 18385-90.
14. Kim HN, Moon JH. Enhanced Photovoltaic Properties of Nb_2O_5-Coated TiO_2 3D Ordered Porous Electrodes in Dye-Sensitized Solar Cells. ACS Appl. Mater. Interfaces. 2012; 4: 5821-25.
15. Lu X, Mou X, Wu J et al. Improved-Performance Dye-Sensitized Solar Cells Using Nb-Doped TiO_2 Electrodes: Efficient Electron Injection and Transfer. Adv. Funct. Mater. 2010; 20 509-15.
16. Wang M, Bai S, Chen A, Duan Y et al. Improved photovoltaic performance of dye-sensitized solar cells by Sb-doped TiO_2 photoanode. Electrochim. Acta. 2012; 77: 54-59.
17. Yang M, Kim D, Jha H et al. Nb doping of TiO_2 nanotubes for an enhanced efficiency of dye-sensitized solar cells. Chem. Commun. 2011; 47: 2032-34.
18. Tian H, Hu L, Zhang C et al. Retarded Charge Recombination in Dye-Sensitized Nitrogen-Doped TiO_2 Solar Cells. J. Phys. Chem. C. 2010; 114: 1627-32.
19. Hafez H, Saif M, Abdel-Mottaleb MSA. Down-converting lanthanide doped TiO_2 photoelectrodes for efficiency enhancement of dye-sensitized solar cells. J. Power Sources. 2011; 196: 5792–96.
20. Im JS, Lee SK, Lee YS. Cocktail effect of Fe_2O_3 and TiO_2 semiconductors for a high performance dye-sensitized solar cell. Appl. Surf. Sci. 2011; 257: 2164–69.
21. Shaikh SMF, Rahman G, Mane R, Joo O. Bismuth oxide nanoplates-based efficient DSSCs: Influence of ZnO surface passivation layer. Electrochim. Acta. 2013; 111: 593-600.
22. An'amt MN, Radiman S, Huang NM et al. Sol–gel hydrothermal synthesis of bismuth–TiO_2 nanocubes for dye-sensitized solar cell. Ceram. Int. 2010; 36: 2215–20.

23. Moula G, Mumin MA, Charpentier PA. Enhancement of Photocurrent in Dye-Sensitized Solar Cells Using Bismuth Doped TiO_2- Graphene as a Hot Carrier Transport. J. Nanomater. Mol. Nanotechnol. (2013), S1:002. doi: 10.4172/2324-8777.S1-002.
24. Leontie L, Caraman M, Visinoiuc A, Rusu GI. On the optical properties of bismuth oxide thin films prepared by pulsed laser deposition. Thin Solid Films. 2005; 4: 230-35.
25. Lafuente B, Downs RT, Yang H, Stone N . The power of databases: the RRUFF project. In: Highlights in Mineralogical Crystallography, T Armbruster and R.M. Danisi, eds. Berlin, Germany, W. De Gruyter, 2015; 4:1-30.
26. Stojanovic BD. Mechanochemical synthesis of ceramic powders with perovskite structure. J. Mater. Process. Technol. 2003; 143/144: 78-81.
27. Ohara S, Kondo A, Shimoda H et al. Rapid mechanochemical synthesis of fine barium titanate nanoparticles. Mater. Lett. 2008; 62: 2957-59.
28. Ruben S. Handbook of the Elements", 8th Printing, Open Court Publishing Company, 1998. ISBN: 0-87548-399-2
29. Peter LM. Dye-sensitized nanocrystalline solar cells. Phys. Chem. Chem. Phys. 2007; 9: 2630-42.
30. Xu Y, Schoonen MAA. The absolute energy positions of conduction and valence bands of selected semiconducting minerals. Am. Mineral. 2000; 85: 543-56.